

Astrometric effects of non-uniform telescope throughput

M. Gai¹ * and R. Cancelliere²

¹*Istituto Nazionale di Astrofisica - Osservatorio Astronomico di Torino, V. Osservatorio 20, 10025 Pino T.se (TO), Italy*

²*Dipartimento di Informatica, Università di Torino, C.so Svizzera 185, 10149 Torino, Italy*

Accepted 2008 September 22. Received 2008 September 22; in original form 2008 August 22

ABSTRACT

In real telescopes, the optical parameters evolve with time, and the degradation is often not uniform. This introduces variations in the image profile and therefore photo-centre displacements which, unless corrected, may result in astrometric errors. The effects induced on individual telescopes and interferometric arrays are derived by numerical implementation of a range of cases. The results are evaluated with respect to the potential impact on the most relevant experiments for high precision astrometry in the near future, i.e. Gaia, PRIMA and SIM, and to mitigation techniques applicable from design stage to calibrations.

Key words: astrometry – telescopes – techniques: image processing.

1 INTRODUCTION

The mirrors of ground based instruments suffer degradation of the reflecting surface, e.g. by oxidation or contamination of the coating, due to dust, moisture and chemical agents in the environments (Vucina et al. 2006). The result is a degradation of the optical throughput, which in general is not uniform, but rather described by a complex, often patchy, distribution. Also, the overall telescope transmission is progressively reduced, so that it becomes necessary to process in particular the primary mirror regularly for removal of the degraded reflecting coating and application of a new one.

Space optics is expected to be much less affected by surface characteristics variations, thanks to the stable environment and suitable protective layers, but degradation e.g. due to γ radiation is still experienced, up to 1% of the overall throughput, depending on the choice of substrate and coating material (Baccaro et al. 2004).

Even small variations are still potentially relevant with respect to high precision astrometric measurements, and as such their effects have been investigated and are discussed in this document. The main experiments in which astrometric errors induced by non-uniform optical throughput variation are potentially relevant are Gaia, PRIMA and SIM.

Gaia (Perryman et al. 2001) is the most important European space mission devoted to micro-arcsec (μas) astrometry currently being implemented. Interferometry also aims at comparable levels of precision by means of both ground based arrays, e.g. the Phase Referenced

Imaging and Microarcsecond Astrometry [PRIMA] facility (Delplancke et al. 2003) of the Very Large Telescope Interferometer [VLTI] of the European Southern Observatory [ESO], or from space, e.g. the Space Interferometer Mission [SIM] (Unwin et al. 2008).

The astrometric performance of an astronomical instrument depends on the detected signal profile. The Point Spread Function (PSF), i.e. the intensity distribution from a point-like object at infinity, is built from the diffraction integral, described in optics textbooks, e.g. Born and Wolf (1985); the numerical implementation used here was described in a previous paper (Gai and Cancelliere 2007). The PSF includes, by a suitable wavefront error (WFE) map, the realistic description of several optical characteristics. The polychromatic PSF is produced by superposition, weighted by spectral distribution, of the monochromatic PSFs.

Hereafter, I_m is the monochromatic PSF at a given wavelength λ , and E_m is the corresponding complex amplitude distribution on the focal plane; F is the effective focal length of the telescope. The coordinates on pupil and focal plane are respectively $\{\xi, \eta\}$ and $\{x, y\}$ (linear units). The complex amplitude depends on the pupil function P and on the aperture transmission function T :

$$E_m(x, y) = k \int d\xi d\eta T(\xi, \eta) \cdot P(\xi, \eta) e^{-i\pi(x\xi + y\eta)/\lambda F}. \quad (1)$$

The constant k provides the appropriate photometric result associated with the source emission, exposure time and collecting area. The monochromatic PSF can be expressed as

$$I_m(x, y) = |E_m(x, y)|^2. \quad (2)$$

The pupil function $P(\xi, \eta) = e^{i\Phi(\xi, \eta)}$ depends on the

* E-mail: gai@oato.inaf.it (MG), cancelli@di.unito.it (RC)

phase aberration function Φ , often expanded e.g. in terms of the Zernike functions Φ_n (Born and Wolf 1985):

$$\Phi(\rho, \theta) = \frac{2\pi}{\lambda} WFE = \frac{2\pi}{\lambda} \sum_n A_n \varphi_n(\rho, \theta). \quad (3)$$

The aperture transmission function T is often considered to take unity value inside the pupil and zero outside; it is therefore used simply as a convenient numerical tool for insertion of the pupil geometric description. In the current simulation, however, it is used also to describe the variation of optical throughput of the telescope throughout the pupil. The formalism is similar to that adopted by Linfield (2004), in the framework of straylight analysis for a Terrestrial Planet Finder (TPF) coronagraph. The most relevant changes are a simplified treatment, since we consider only transmission variations and neglect phase contributions, and the focus on astrometric effects, i.e. image photo-centre displacements.

We expect that a uniform variation of the optical throughput over the whole telescope aperture does not introduce any variation on the image photo-centre; however, for a generic aberrated configuration, a non-uniform pupil transmission introduces an amplitude modulation of the pupil function, thus modifying the resulting focal plane energy distribution, hence the measured signal profile, and consequently its photo-centre estimated position. Such photo-centre displacement is associated with an error on the astrometric measurement. Although in general the optical throughput is wavelength dependent, our analysis is referred to a single spectral type source, and uniform spectral dependence is assumed. Further levels of detail may be introduced in future investigations.

In section 2 we discuss the introduction of transmission non-uniformity features and evaluate a set of reference cases focused on the astrometric performance of one telescope. In section 3 we analyse some consequences on the measurements of an interferometric array. Then, in section 4, we discuss the implications of our findings on design and calibration of astrometric instruments. Finally, we draw our conclusions.

2 SINGLE TELESCOPE

The analysis is focused on a configuration similar to the Gaia telescope optics and operation, also because its rectangular geometry is marginally more convenient for numerical simulation. The primary mirror size is 1.45×0.45 m; the effective focal length is $EFL = 35$ m, resulting in an optical scale of 5.89 arcsec/mm. For simplicity, the study case in this document is one-dimensional; this is also most immediately related to the Gaia elementary measurements. The PSF is integrated in the direction not used for the astrometric measurement by binning on the CCD detector; this is simulated by numerical integration over an appropriate region. Also, some of the effects associated with the instrument characteristics and operations are included in the form of equivalent effects on the PSF through the corresponding Modulation Transfer Function (MTF); in particular, this includes the detector pixel (size $10 \times 30 \mu\text{m}$) and Time Delay Integration (TDI) readout (Gai et al. 1998). The values used are

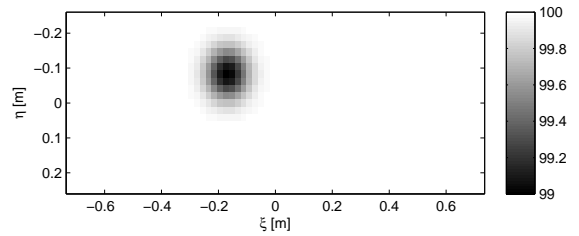


Figure 1. Throughput distribution (in percent) for a selected patch position. The transmission is reduced locally by $\leq 1\%$.

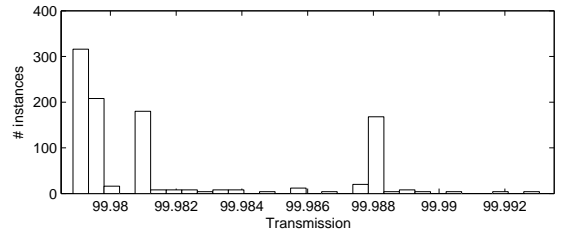


Figure 2. Histogram of throughput (in percent) vs. patch position ranging over the telescope pupil.

representative of the Gaia nominal configuration and operation.

The optical throughput perturbations described below are applied to a range of cases with different image quality, achieved by selection of the 21 lowest order Zernike coefficients, corresponding to the normalised radius raised up to the fifth power, as in the table included in Gai and Cancelliere (2005). The optical images are generated as pseudo-polychromatic, using a central wavelength of 617 nm, with weight 100%, and two side wavelengths at ± 100 nm, with weight 50%, approximating the instrument response to a blackbody source at $T = 3 \times 10^4$ K. The photo-centre estimation is performed using the centre of gravity algorithm, as it is simple and independent of signal models.

2.1 Opacity patches

The telescope throughput degradation is introduced as a localised reduction with respect to the nominal unity value ($T_0 = 1$), i.e. an opacity patch p , so that the local transmission over the pupil is $t(\xi, \eta) = T_0 - p(\xi, \eta)$. A Gaussian shape of the opacity patch is adopted, with given characteristic size σ ($\sigma = 5$ cm for most of the cases below), peak position $\{\xi_0, \eta_0\}$ and peak value p_0 :

$$p(\xi, \eta) = p_0 \cdot \exp \left[-\frac{(\xi - \xi_0)^2 + (\eta - \eta_0)^2}{2\sigma^2} \right]. \quad (4)$$

For all cases investigated, the peak value is set to $p_0 = 1\%$, i.e. the perturbed telescope transmission ranges between 99% and 100% of the unperturbed value. The opacity distribution is therefore not normalised, and its area is $A_p = 2\pi\sigma^2$. A selected case corresponding to patch position close to the centre of the pupil is shown in figure 1. The overall optical throughput variation can be expected to be dependent on the peak and size of the opacity distribution, i.e. of order of $p_0 \cdot A_p / A_T$, where $A_T = L_\xi L_\eta$

is the primary mirror area. For a generic centre position, part of the patch is outside the pupil, further reducing the throughput degradation. The overall transmission variation, averaged over the pupil, is thus well below 0.1%, because the opacity patch is much smaller than the primary mirror size. Thus, photometric measurements are affected by marginal degradation.

2.2 Simulation

The position of the opacity patch is translated uniformly over 100 positions on the long side of the telescope, and over 10 positions on the short side; each case is thus evaluated on a total number of 1000 instances. The pupil and focal plane sampling resolution is respectively 2×2 cm and $2 \times 6 \mu\text{m}$. An histogram of the transmission distribution is shown in figure 2. The throughput mean value over the sample of patch positions is 0.99982, with standard deviation 3×10^{-5} . Hereafter, a range of WFE cases is evaluated against the set of throughput perturbations described above. In all cases, the readout area is set to 12×12 pixels.

2.2.1 Case 1

A set of random values of the 21 lowest order Zernike coefficients is selected, with normal distribution and peak value of 50 nm. The corresponding WFE has RMS value of 35.05 nm, corresponding to a fairly good optical quality, $\sim \lambda/20$ at $\lambda = 700$ nm. The WFE distribution over the pupil is shown in figure 3 (top). The photo-centre computed on each instance of opacity patch position is affected by displacements with respect to the unperturbed case; its distribution vs. opacity patch position is shown in figure 3 (mid). The photo-centre displacement mean and RMS are respectively 0.03 and $3.34 \mu\text{as}$; the peak-to-valley (PTV) is $14.13 \mu\text{as}$.

2.2.2 Case 2

In order to evaluate the dependence on the amount of aberration, the WFE shape is retained, but its amplitude is reduced by a factor two by halving all Zernike coefficients. The resulting RMS WFE is thus reduced to 17.53 nm; the map is not shown here, since with respect to figure 3 (top) only the scale changes, by a factor two. The photo-centre distribution is similar to that from case 1 (figure 3, mid), but it is also reduced by a factor two; the mean and RMS are respectively 0.02 and $1.67 \mu\text{as}$; the PTV is $7.09 \mu\text{as}$. The photo-centre discrepancy between case 1 and case 2, after multiplication of the latter by a factor two, have mean and RMS respectively zero and $0.03 \mu\text{as}$.

2.2.3 Case 3

Similarly, in case of larger aberration with the same shape (achieved by multiplication by a factor two of the Zernike coefficients, resulting in RMW WFE = 70.11 nm), the photo-centre displacement is doubled, but again similar to that of case 1 (figure 3, mid). The mean and

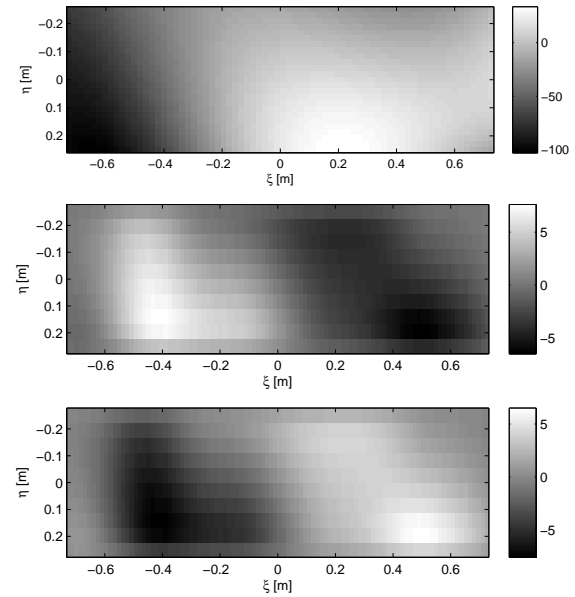


Figure 3. Map of WFE for case 1 (top, in nm); distribution of photo-centre (in μas) vs. opacity patch position, case 1 (mid) and 4 (bottom, aberration reversed in sign).

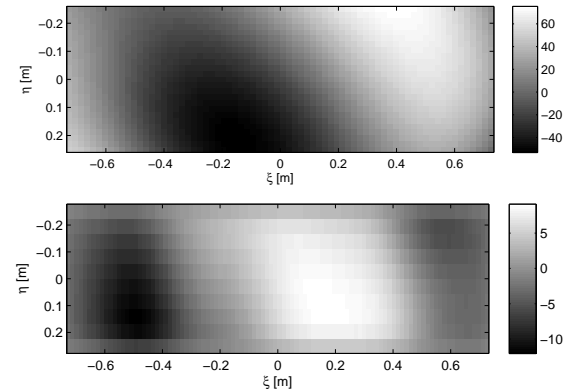


Figure 4. Realistic WFE selected for case 6 (top) and the corresponding distribution of photo-centre (in μas) vs. patch position (bottom).

RMS photo-centre displacement are respectively 0.07 and $6.67 \mu\text{as}$; the PTV is $27.92 \mu\text{as}$. The photo-centre discrepancy between case 1 and case 3, after division of the latter by a factor two, have mean and RMS respectively zero and $0.09 \mu\text{as}$.

2.2.4 Case 4

In case of symmetric aberration, i.e. changing the sign of the Zernike coefficients, the same RMS WFE is retained, and the focal plane image is symmetric with respect to case 1. Correspondingly, the photo-centre displacement, shown in figure 3 (bottom), is opposite to the initial distribution of case 1: the mean and RMS are respectively -0.03 and $3.34 \mu\text{as}$; the PTV is $14.13 \mu\text{as}$. The photo-centre discrepancy between case 1 and case 4, after sign

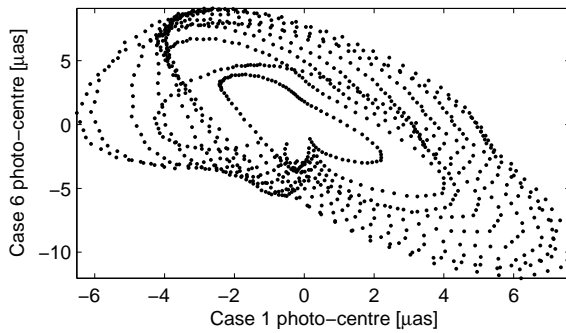


Figure 5. Photo-centre distribution (in μas) of case 6 with respect to case 1. Different WFE distributions induce quite different astrometric errors.

reversal of the latter, have both mean and RMS equal to zero within 10^{-6} μas .

2.2.5 Case 5

The diffraction limit case is also worth considering, because the throughput non-uniformity introduces an asymmetry in the system, which is no longer ideal. This potentially might result in a photo-centre displacement. The simulation shows that this is not the case, since the photo-centre mean, RMS and PTV values are all zero. This is consistent with the mathematical framework of the diffraction integral, since replacing in Equation 1 the null aberration $\Phi = 0$, a unity pupil function is achieved, and we can see that sign reversal on the focal plane coordinates only introduces a global phase inversion on the complex argument, which vanishes in the square modulus providing an invariant intensity distribution (Equation 2). Besides, in mathematical terms, the Fourier transform $F(\omega)$ of a real function $f(t)$ is hermitian, so that $F(-\omega) = F^*(\omega)$ (complex conjugate), with the same result.

2.2.6 Case 6

In order to test a different shape of aberration, an alternate set of Zernike coefficients is generated, in the same range of values, with a resulting RMS WFE of 35.23 nm. The same opacity patch distribution as above is used. The WFE distribution is shown in figure 4 (top); it is equivalent in terms of RMS value, but different in shape, to that of case 1 (figure 3, top). The photo-centre displacement distribution, shown in figure 4 (bottom), has not only different shape with respect to that derived from the previous WFE distribution, but also larger deviations from the unperturbed case: the mean and RMS are respectively 0.13 and 5.45 μas ; the PTV is 21.14 μas . The plot of photo-centres of cases 1 and 6 against each other, shown in figure 5, in which each point is affected by the same opacity patch, does not evidence significant correlations. The RMS WFE is therefore not in itself a sufficient indication of the instrument sensitivity to non-uniform throughput variations.

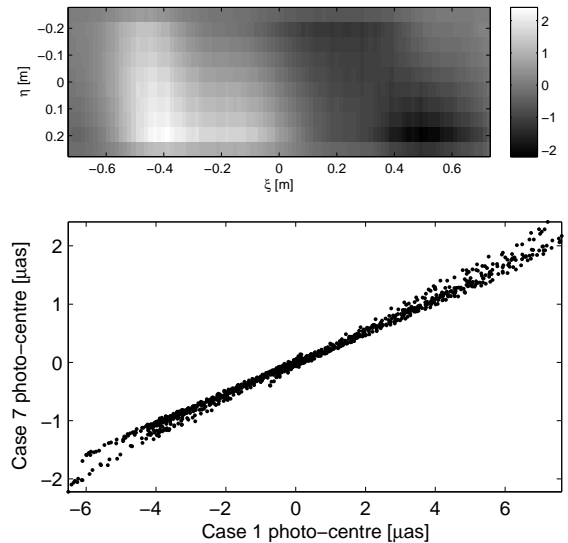


Figure 6. Distribution of photo-centre (top, in μas) vs. patch position, case 7 (smaller patch), and photo-centre distribution (bottom, in μas) of case 7 with respect to case 1.

2.2.7 Case 7

In this case, the characteristic size of the Gaussian distribution of opacity is reduced by a factor two, to $\sigma = 2.5$ cm. Since the peak value remains set to 1%, the effective perturbation to the system is smaller, and a reduced astrometric effect can be expected. The photo-centre displacement distribution, shown in figure 6 (top), is consistent with this expectation: the mean and RMS are respectively 0.00 and 0.93 μas ; the PTV is 4.63 μas . The photo-centre plot of case 7 vs. 1, shown in figure 6 (bottom), does evidence a significant correlation, since for each point the two cases have in common both the opacity patch and the WFE map. Scaling the former by a factor 3.56, defined by best fit, the discrepancy mean and RMS are respectively 0.02 and 0.29 μas . The scaling factor is close, but not equal, to the ratio of the opacity patch areas (i.e. four) on the pupil plane; given the non-linearity of the diffraction integral, Eqs. 1 and 2, this seems to be reasonable.

2.3 Comparison

The various WFE cases are associated with different photo-centre displacements, induced by the same set of telescope throughput perturbations. A compact representation of the relationship among the first four cases is shown in figure 7. The image profile is more aberrated in case 3 than in cases 1 and 2, and correspondingly a larger fraction of the total flux falls outside the readout region; this introduces additional noise. The astrometric error induced by a given transmission perturbation, if the WFE distribution is uniformly scaled by a factor 0.5, 2, and -1, is with good approximation multiplied by the same amount.

Independent WFE distributions induce quite different astrometric errors, with respect to the same transmission perturbation, as shown in figure 5. Thus, the photo-

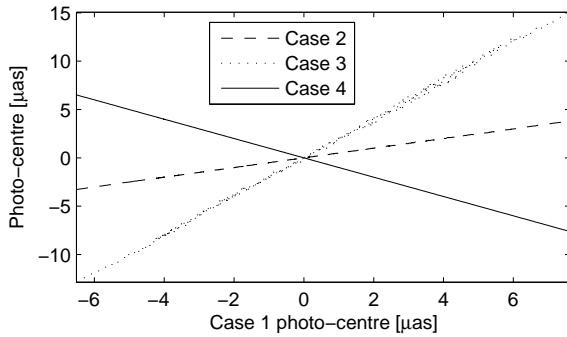


Figure 7. Photo-centre distribution (in μas) of cases 2, 3 and 4 with respect to case 1. Scaling the WFE amplitude induces a proportional change in the resulting astrometric error.

centre displacement depends on the focal plane position.

3 INTERFEROMETRY

The opacity patch representing the non-uniform optical throughput of a telescope also has an impact on the performance of an interferometer. The orientation and phase distribution of the compressed beam is affected as derived in Sec. 2, and this will contribute to the error budget of visibility and phase determination, depending on implementation aspects of the transport and combination optics (Buscher et al. 2008). Additionally, a specific contribution to *baseline noise* can be identified.

An effective pupil centre position can be defined for each opacity patch, as average weighted by the transmission distribution:

$$\xi_p = \frac{\int d\xi d\eta \xi \cdot t(\xi, \eta)}{\int d\xi d\eta t(\xi, \eta)} = \xi_0 \frac{p_0}{T_0} \frac{A_p}{A_T - A_p}. \quad (5)$$

where A_p and A_T are the patch and primary mirror areas.

Thus, the pupil centre displacement is related to the position of the opacity patch, weighted by the relative opacity vs. unperturbed transmission, and by the relative size of the patch vs. pupil.

The opacity patch centre position ξ_0 can range over the whole geometric extension of the pupil, with uniform distribution, so that the average pupil displacement is zero:

$$\langle \xi_p \rangle = \int d\xi d\eta \xi_p \equiv 0, \quad (6)$$

and its RMS value is related to the RMS pupil size:

$$\sigma^2(\xi_p) = \langle (\xi_p - \langle \xi_p \rangle)^2 \rangle = \frac{p_0}{T_0} \frac{A_p}{A_T - A_p} \xi_{RMS}^2. \quad (7)$$

In simple geometry cases, the RMS size of the aperture can be easily expressed in terms of the linear size L_ξ in the relevant direction, for a rectangular pupil, or of the diameter D , for a circular unobstructed pupil, i.e. respectively $\xi_{RMS} = L_\xi/\sqrt{12}$ and $\xi_{RMS} = D/4$.

Non-uniform variations of the optical throughput, therefore, induce apparent changes in the position of each telescope of an interferometric array.

Let us consider the case of a two telescope interferometer with baseline B , observing a pair of stars with separation $\varphi \ll 1$ rad and zenithal distance θ (for the object with higher elevation), in a planar geometry for convenience. The variation of optical path difference (OPD) between the two stars, measured by the interferometer, is then $\Delta OPD \simeq \varphi B \cos \theta$, so that the baseline error $\sigma(B) = \sigma(\xi)$ is reflected into an astrometric error $\sigma(\varphi)$ on the determination of the star separation φ :

$$\sigma(\varphi) = \varphi \frac{\sigma(B)}{B}. \quad (8)$$

Such effects are relevant e.g. for orbit determination, when measurements taken at different epochs t_1, t_2 are combined; in the mean time, the instrument may have suffered changes not easily identified (e.g. $< 1\%$ in optical throughput) but sufficient to introduce relevant astrometric errors. We can evaluate the magnitude of the effect on two cases, namely PRIMA at the ESO VLTI (ref. PRIMA) and SIM.

3.0.1 PRIMA

The baseline is of order of 100 m, and the stellar separations considered for high precision astrometry in K band ($2.2 \mu\text{m}$) are up to a few tens of arcsec. We consider a measurement performed by means of the Auxiliary Telescopes (AT, diameter 1.8 m), and assume one opacity patch with 1% throughput degradation and size $\sigma = 5$ cm, in an arbitrary position over the pupil. Then, the RMS baseline error is about 3.5 mm, and the corresponding error for baseline $B = 100$ m and separation $\varphi = 10''$ is $\sigma(\varphi) = 35 \mu\text{as}$.

3.0.2 SIM

The baseline is $B = 6$ m and the operating wavelength is in the visible, so that we select $\lambda = 600$ nm; the individual apertures have diameter $D = 0.3$ m. Narrow angle astrometry is performed on separations up to $\varphi = 1^\circ$, so that, assuming an opacity patch with 1% throughput degradation and size $\sigma = 1$ cm, we get a RMS baseline error of 0.7 mm and angular measurement error of $\sigma(\varphi) = 0''.4$.

The larger astrometric error with respect to the PRIMA VLTI case is due to the combined contributions of shorter baseline and larger separation angle.

3.1 Calibration vs. metrology

The above values of error introduced by non-uniform transmission variation are not immediately related to the final measurement performance, because diagnostics and correction are not yet considered. Of course, on-sky calibration procedures are foreseen, both for PRIMA and for SIM, in which the instrument is rapidly switched between the science target and suitable reference objects. The errors discussed above are systematic and strictly correlated (although not equal) among different sources, and this is a key factor in the definition of a measurement sequence leading to their suppression. Depending

on availability of specific calibrators (e.g. binary systems or resolved objects considered sufficiently stable), simple calibration sequences can be devised.

For example, if φ_1 and φ_2 are the angular quantities of interest referred to the science and reference sources, respectively, the measurement of the latter changes between epochs t_1, t_2 only because of instrument variation by $\sigma(\varphi_2)$, i.e. $\varphi_2(t_2) = \varphi_2(t_1) + \sigma(\varphi_2)$, whereas the former changes by both astrophysical and instrument amounts, respectively $\delta\varphi_1$ and $\sigma(\varphi_1)$: $\varphi_1(t_2) = \varphi_1(t_1) + \delta\varphi_1 + \sigma(\varphi_1)$. From Equation 8, instrumental errors are correlated:

$$\sigma(\varphi_1) = \sigma(\varphi_2) \frac{\varphi_1}{\varphi_2}, \quad (9)$$

so that the set of measurements allows correct determination of the desired astrophysical quantity $\delta\varphi_1$.

In practice, the calibration procedure must be more complex, because the systematic errors affecting the measurement are likely to include additive components, as well as multiplicative components as from Equation 8.

It should be noted that a metrology system installed to monitor the distance among fiducial points on the telescope structure is not sensitive to effective pupil displacements induced by non-uniform throughput variations, because the change involves optical parameters and not the instrument geometry. Metrology can be extremely useful with respect to short term metrology disturbances from the environment, and to long term geometry perturbations, but is liable to failure in the detection of the effects discussed herein.

4 DISCUSSION

The astrometric effects induced by non-uniform variations of the telescope throughput depend of course on the characteristic size and amplitude of the defects on the mirror surfaces. In turn, they depend on details of manufacturing and operating environment which are not easily identified nor measured. Useful practical indications may be provided by testing representative components e.g. during or after a significant period passed within an environment comparable to that of operation, as a cryogenic vacuum chamber, and subject to the expected radiation doses, as in Baccaro et al. (2004).

4.1 Design and implementation aspects

For future astrometric instruments, using a comparably large field of view, the balancing of errors due to symmetric aberrations could be used to advantage, allowing compensation over a set of measurements taken in suitable conditions (i.e. cases 1 and 4 above). An aberration control approach could be conveniently adopted at the early design stage, minimising the sensitivity to manufacture tolerancing and alignment errors, also with particular regard to the optimisation criteria of in-orbit re-alignment, to preserve the symmetry. From a strictly experimental standpoint, it is possible to devise conceptual schemes for throughput measurement devices to be used on ground, for performance verification during the instrument integration, and even in orbit, to monitor the

in-flight response. Their cost and benefit with respect to purely astronomical calibration is a matter of project trade-off.

4.2 Impact on Gaia

For Gaia, a significant fraction of the astrometric effect associated with the image shape evolution induced by telescope throughput non-uniform variation *could* be taken care of within the framework of the self-calibration process, assuming that the instrument variation is sufficiently small over a time scale comparable with the coverage of the whole sky or a large part of it, e.g. order of six months. Also, part of the error may be averaged down among subsequent measurements, thus resulting in partial compensation.

Partial compensation can be achieved also in case of symmetric aberrations over the field of view, as discussed in Busonero et al. (2006) on the subject of chromatic astrometric errors. If opposite regions on the focal plane are affected by aberrations with opposite sign (as in cases 1 and 4 above), the astrometric errors introduced on the two measurements cancel out. Also in case of partial symmetry, or of limited balancing of the aberrations over the focal plane, some compensation can be achieved.

Since the aberration distribution (and image profile) change over the focal plane, independently for each telescope, non-uniform throughput variations introduce astrometric errors in the large angle measurement. The distribution of photo-centre displacements in case of different WFE, as in figure 5, can provide an indication of the effect amplitude, but it is not fully representative because the patch positions are not correlated between the telescopes. The result is a field dependent error on the base angle, which is not strictly correlated to the measurements from the Base Angle Monitoring device (BAM), which probes only a small region of each optical system.

An indication of throughput variation could be achieved by evaluation of the photometric response over a significant set of bright stars during each period of observation, in order to monitor the instrument response at the sub-milli-mag level (corresponding to 0.01% overall transmission variation). However, photometry is not sufficient *per se* to provide adequate information, since it cannot distinguish the cases of uniform and non-uniform variation over the aperture.

A wavefront sensor (WFS) of the Hartman-Shack type, splitting the collimated beam in several smaller regions, is potentially able to provide information on the variation of instrument transmission over its pupil, by photometric monitoring of the intensity from each region, as well as WFE derivative diagnostics by the elementary image displacements on the focal plane. However, a WFS is sensitive also to the variations of the non-common part of the system, namely the geometry and response of the lenslet array. As for photometry based diagnostics, the detector might also suffer changes which should be identified and factored out from the estimate of optical throughput variation.

Besides, since the astrometric effect is associated with a variation of the effective signal profile, suitable

image descriptors may be monitored, which usually have magnitude dependent sensitivity (e.g. image moments). The development of diagnostic tools based on image profile variation (Gai and Cancelliere 2005) might prove useful to identification of critical instrument changes, in support to the previous approaches.

Future investigations might tackle the development of efficient monitoring and correction algorithms, based on the available information, as well as the investigation of cumulative and field-dependent astrometric effects associated with the evolution of the telescope throughput.

5 CONCLUSION

Non-uniform variations of the optical throughput over the telescope aperture, as experienced in ground based instruments, may provide astrometric effects significant at the level of several microarcseconds. This may in turn represent a non negligible contribution to the error budget of the most challenging astrometric experiments currently under implementation or proposed for the near future, as Gaia, PRIMA and SIM.

The scale of the effects depends on manufacturing and operation parameters not easily measurable at the relevant level, i.e. order of 1% on mirror reflectivity over regions of few cm, or 0.02% on global throughput. Procedures of periodic calibration on sky can be used to retain acceptable levels of the systematic errors introduced by instrument response variations, in particular for long term measurements as interferometric orbits.

For Gaia, the time scale of instrument evolution must be compared with the period of effective parameter calibration, to verify that the systematic errors are adequately removed from the data. Information from the WFS and from photometry might be exploited to monitor astrometric effects, as well as diagnostics of the image profile evolution.

ACKNOWLEDGMENTS

The analysis of interferometric effects was performed in the framework of the project PRIN INAF 2007 no. 6.

REFERENCES

- Baccaro S., Cecilia A., Di Sarcina I., Piegari A., 2004, Proc. SPIE, 5494, 529
 Born M., Wolf E., 1985, Principles of optics, Pergamon, New York
 Buscher D.F., Baron F., Haniff C.A., Young J., 2008, Proc. SPIE, 7013, 7013-48
 Busonero D., Gai M., Gardiol D., Lattanzi M.G., Loreggia D., 2006, A&A, 449, 827
 Delplancke F., Derie F., Paresce F., Glindemann A., Lévy F., Lévêque S., Ménardi S., 2003, AP&SS 286, 99
 Gai M., Casertano S., Carollo D., Lattanzi M.G., 1998, PASP 110, 848
 Gai M., Cancelliere R., 2005, MNRAS, 362, 1483

- Gai M., Cancelliere R., 2007, MNRAS, 377, 1337
 Linfield R.P., 2004, Proc. SPIE, 5487, 1255
 Perryman M.A.C., de Boer K.S., Gilmore G., Høg E., Lattanzi M.G., Lindegren L., Luri X., Mignard F., Pace O., de Zeeuw P.T., 2001, A&A, 369, 339
 Unwin S.C., Shao M., Tanner A.M. et al., 2008, PASP, 863, 38
 Vucina T., Boccas M., Araya C., Ahhee C., 2006, Proc. SPIE, 6273, 62730W